6/14/95

SANDIA REPORT

SAND90–2318 • UC–920
Unlimited Release
Printed May 1995

Deformation Study of Separator Pellets for Thermal Batteries

Ronald A. Guidotti, Frederick W. Reinhardt, Edward V. Thomas

Prepared by
Sandia National Laboratories
Albuquerque, New Mexico 87185 and Livermore, California 94550
for the United States Department of Energy
under Contract DE-AC04-94AL85000

Issued by Sandia National Laboratories, operated for the United States Department of Energy by Sandia Corporation.

Available to DOE and DOE contractors from
Office of Scientific and Technical Information
PO Box 62
Oak Ridge, TN 37831

Prices available from (615) 576-8401, FTS 626-8401

Available to the public from
National Technical Information Service
US Department of Commerce
5285 Port Royal Rd
Springfield, VA 22161

NTIS price codes
Printed copy: A04
Microfiche copy: A01

DISCLAIMER

Portions of this document may be illegible in electronic image products. Images are produced from the best available original document.

SAND90-2318
Unlimited Release
Printed May 1995

Distribution
Category UC-920

Deformation Study of Separator Pellets for Thermal Batteries

Ronald A. Guidotti and Frederick W. Reinhardt
Battery Research Departtment

Edward V. Thomas
Statistics, Computing, and Human Factors Department
Sandia National Laboratories
Albuquerque, New Mexico 87185-5800

Abstract

The deformation characteristics of pellets of electrolyte-binder (EB) mixes based on MgO were measured under simulated, thermal-battery conditions. Measurements (using a statistically designed experimental strategy) were made as a function of applied pressure, temperature, and percentage of theoretical density for four molten-salt electrolytes at two levels of MgO. The EB mixes are used as separators in Li-alloy thermal batteries. The electrolytes included LiCl-KCl eutectic, LiCl-LiBr-KBr eutectic, LiBr-KBr-LiF eutectic, and a LiCl-LiBr-LiF electrolyte with a minimum-melting composition. The melting points ranged from 313°C to 436°C. The experimental data were used to develop statistical models that approximate the deformation behavior of pellets of the various EB mixes over the range of experimental conditions we examined. In this report, we discuss the importance of the deformation response surfaces to thermal-battery design.

Contents

Appendices

Figures

Tables

Deformation Study of Separator Pellets for Thermal Batteries

Introduction

Thermally activated batteries use a molten-salt electrolyte that serves as a separator between the anode [e.g., Li(Si)] and the cathode (e.g., FeS_2) of each cell. When the battery is activated, a pyrotechnic heat source raises the temperature of each cell above the melting point of the electrolyte (352°C for the LiCl-KCl eutectic) and allows current to be drawn from the battery.

The electrolyte is typically immobilized by using an inert oxide binder, such as MgO powder, that is thermodynamically stable to the Li and Li-alloy anodes used in the batteries. The electrolyte-binder (EB) mixes are prepared by blending together the MgO and the electrolyte powders and by fusing the material above the melting point of the electrolyte (typically, for up to 16 h). After granulation, the EB powder is pressed into separator pellets. A cross-sectional representation of a typical thermal cell is shown in Figure 1.

The mechanical properties of the separator pellet are important for proper operation of thermal batteries. If there is excessive deformation (plastic flow) of the pellet when the electrolyte is molten, intracell shorting can occur with thin cells if the anode and cathode pellets come into contact. In addition, electrolyte leakage can occur, leading to intercell parasitic currents as the electrolyte dewets the MgO and wicks into the ceramic blanket wrap used to insulate the battery.

On the other hand, if there is insufficient deformation, unacceptable wetting of the anode and cathode pellets by the molten separator pellet can occur. This can lead to a high electrical resistance at the separator-anode and separator-cathode interfaces during discharge, and thus can adversely impact performance.

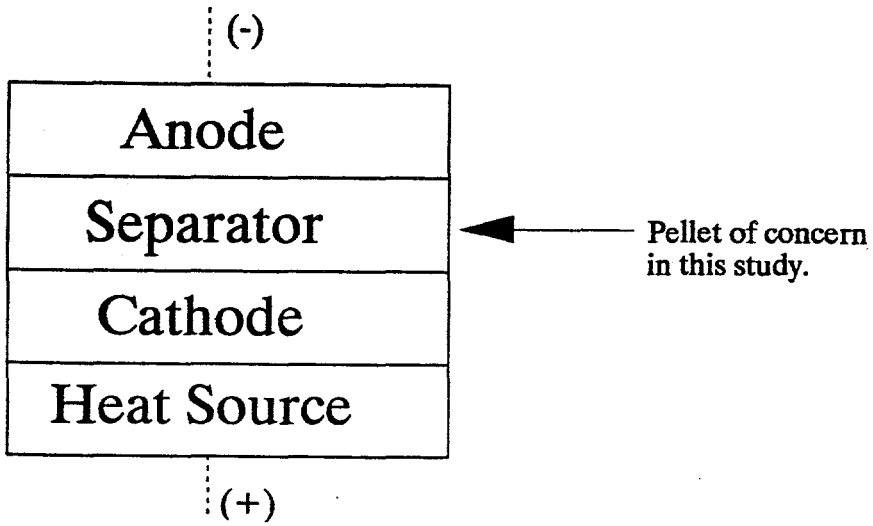

Figure 1. Cross-Sectional Representation of a Thermal Cell

Factors that influence the deformation properties of the separator pellet include the MgO content, the applied (stack) pressure, the temperature, and the percent of theoretical density (porosity). In the past, an applied pressure of 14.3 psig (99 kPa), a temperature of 530°C, and a nominal density of 75% of theoretical were used as test levels for measuring the deformation of separator pellets.[1] However, the relative sensitivity of the deformation to these test levels was unknown. Therefore, a study was undertaken to examine the effect of the above factors on the deformation properties of separator pellets made from EB mixes formulated with four different electrolytes:

- the standard LiCl-KCl eutectic
- a low-melting LiCl-LiBr-KBr eutectic
- a low-melting LiBr-KBr-LiF eutectic
- an all-Li electrolyte (LiCl-LiBr-LiF minimum-melting composition).

For each electrolyte type, an experimental strategy was developed to facilitate an understanding of the individual and interactive effects of the various factors on deformation. Analysis of the resulting experimental data led to the development of response-surface plots that relate the deformation to the levels of the experimental factors.

Experimental Procedures

Materials

Electrolytes - Reagent-grade halide salts were used in the preparation of the various electrolytes. The compositions of the four electrolytes used and their melting points are summarized in Table 1.

The individual halide salts were vacuum dried at 100°C for 40 h before use. The appropriate amounts of the salts were blended for each electrolyte composition and the mixes were fused at 650°C for 3 h. After quenching on an Inconel tray, the salts were pulverized to -325 mesh using a Mikro-Pulverizer (Mikropul, Summit, NJ).

EB Mixes - The EB mixes were prepared by blending the electrolyte and MgO powders together using Freon TF®.[4] Before blending, the MgO was first baked at 600°C for 4 h to decompose carbonates and hydroxides of Mg. The EB mixes were heated in a 35°C convection oven to remove the Freon TF. Except for the all-Li EB mix, which was fused at 500°C for 16 h, the EB mixes were then fused at 400°C for 16 h. After fusion, the EB mixes were granulated to -60 mesh prior to pelletizing the separator discs to the desired densities. The theoretical densities (TDs) were calculated using the densities of the individual components, assuming additivity of volumes. After pressing, the separator pellets were vacuum dried at 100°C for 16 h.

All the separator pellets in this study were 3.28 cm (1.25 in) in diameter and 0.150 cm (0.0591 in) thick. The masses of the pellets were adjusted to obtain the desired % TD for these dimensions.

All material processing and handling and all deformation testing were conducted in a dry room maintained at <300 ppm water vapor (<1% relative humidity).

Table 1. Electrolytes Evaluated in Separator Study

Name	Electrolyte Composition, w/o	*Melting Point, °C
Standard	55 KCl/45 LiCl	352
LM#1**	51.41 KBr/36.54 LiBr/12.05 LiCl	321
LM#2	57.33 LiBr/42 KBr/0.67 LiF	313†
All-Li	68.4 LiBr/22 LiCl/9.6 LiF	437

*As determined by differential scanning calorimetry in this laboratory
**LM designates "low melting."
†This electrolyte was reported as having a melting point of 280°C. (See Reference 2). This composition was subsequently found to be slightly off eutectic during subsequent work at Sandia National Laboratories (SNL) and at Argonne National Laboratory (ANL). (See Reference 3.)

Deformation Tester

The experimental setup used for deformation testing of the separator pellets was identical to that used for characterizing catholyte pellets for $Ca/CaCrO_4$ thermal batteries.[5] Basically, the setup consisted of a single-cell tester fitted with a linear variable differential transformer (LVDT) to monitor the change in the thickness of the pellet during the test. The applied pressure to the separator pellet was changed by adjusting the mass of the weight attached to the ram of the tester.

Statistical Experimental Design

The test matrix used for this study is summarized in Table 2. Except for the % MgO, each of the experimental factors was tested at three levels, for 3^3 or 27 experiments per each EB composition. Normally, the lowest nominal % TD was 65, although values as low as 55 were used in several instances. Three pellets were tested at each test condition and the mean deformation and standard deviation were determined.

The selected ranges of factor levels were based on previous studies and physical constraints. The lower TD limit was determined by the fragility of the separator pellet. Because electrolyte leakage becomes excessive at TDs above 90%, the upper limit was maintained below this level.

The temperatures chosen are those that span the typical operating range of a normally functioning thermal battery. The levels of MgO chosen for each electrolyte were determined in earlier empirical studies with these materials.[6] The lower applied pressure is typical of those measured in stack-relaxation experiments with $Li(Si)/FeS_2$ thermal batteries. The upper pressure limit was determined by the total mass that could be handled by the deformation tester for the size of the separator pellet used in the study.

Statistical Analysis and Modeling

The percent reduction in separator pellet thickness was not modeled directly as a function of the experimental factors. Instead, the logit transformation of the percent reduction in thickness was modeled. The logit-transformed percent reduction in thickness is $\ln[Y/(100-Y)]$, where Y is the mean percent reduction in thickness. In gen-

Table 2. Experimental Factors and Associated Levels

Factor	Levels
% Theoretical Density (Nominal)	65, 75, 85
Temperature, °C	500, 530, 560
Applied Pressure, psig (kPa)	14.4 (99), 23.8 (157), 32.8 (226)
% MgO	
a. Standard. Electrolyte	35, 40
b. LM#1 Electrolyte	30, 35
c. LM#2 Electrolyte	25, 30
d. All-Li Electrolyte	30, 35

eral, the models considered are subsets of the complete quadratic model:

$$\ln[Y/(100-Y)] = b_0 + b_1P + b_2T + b_3D + b_{12}PT + b_{13}PD + b_{23}TD + b_{11}P^2 + b_{22}T^2 + b_{33}D^2 + e \quad [1]$$

where:

P = applied pressure (psig)

T = temperature (°C)

D = % TD

the b_i's and b_{ij}'s are model parameters to be estimated and *e* is a random error.

The b_{ij} term relates to the magnitude of the interaction between the *i*th and *j*th factors; i.e., the combined effect of these factors that is in addition to the simple effect b_i and b_j. (Pressure units of psig were used for modeling purposes, rather than kPa, because thermal-battery design engineers normally use these units.)

The purpose of the logit transformation was to make the errors (*e*'s) symmetric and to equalize the variance of *e* over the range of Y. For a given mixture, the model selected was the one with the fewest acceptable number of terms that fit the experimental data. Table 3 shows the model terms included for each mixture. All models included the b_0 term (intercept)

For example, for the EB mixtures with LM#1 or LM#2 electrolytes, the models selected were of the form:

$$\ln [Y/(100-Y)] = b_0 + b_1P + b_2T + b_3D + b_{13}PD + b_{33}D^2 + e \quad [2]$$

The parameters associated with each model (e.g., b_0, b_1,b_2, b_3, b_{13}, and b_{33} for the LM#1 and LM#2 electrolytes) were estimated by weighted least-squares regression. In order to avoid numerical problems during the computation of the parameter estimates (frequently present for polynomial regression analysis), the study factors were centered and scaled as follows:

Table 3. Terms Used for Modeling Deformation Data

Electrolyte	% MgO in EB	Model Terms Included
LiCl-KCl Electrolyte	35	P D PD P^2 D^2 $(PD)^2$
LiCl-KCl Electrolyte	40	P D
LM#1 Electrolyte	25	P T D PD D^2
LM#1 Electrolyte	30	P T D PD D^2
LM#2 Electrolyte	25	P T D PD D^2
LM#2 Electrolyte	30	P T D PD D^2
All-Li Electrolyte	30	P T D PD P^2 D^2
All-Li Electrolyte	35	P T D PD P^2 D^2

$T^* = (T-530)/30$, $P^* = (P-23.8)/10$,

and $D^* = (D-70)/20$. [3]

Weighted least-squares regression gives weight to each measurement triplet that depends on the mean and standard deviation of the three measurements. The weights (w_i's) associated with the ith experimental conditions are defined as

$w_i = [Y(100-Y)]^2$ for $S < 1$ [4a]

or $w_i = [Y(100-Y)/S]^2$ for $S>=1$. [4b]

where Y and S are the average and standard deviation, respectively, of the three measurements of the percent reduction in thickness. For a fixed standard deviation, S, the weight is maximized when Y = 50%.

The data from the deformation tests were analyzed using PROC Reg in SAS.[7] DISSPLA (on a VAX platform) was used to produce the contour plots that appear in this report.[8] Currently, a number of software packages for contour plotting are now available for use with a PC. These include Axum (TriMetrix, Seattle, WA), Surfer (Golden Software, Golden, CO), Design Expert (Stat-Ease,Inc., Minneapolis, MN), TechPlot (Polysoft, Salt Lake City, UT), and Minitab (Minitab, Inc., State College, PA).

Results

LiCl-KCl (Standard) Electrolyte: 35% MgO

A typical deformation profile for a separator pellet formulated with LiCl-KCl eutectic and 35% MgO and pressed to 75% TD is shown in Figure 2 for a temperature of 530°C and an applied pressure of 14.4 psig (99 kPa).

The change in pellet thickness (slumping) was almost instantaneous once the electrolyte melted. (This behavior was found to be uniform for all the EB mixes evaluated, regardless of the electrolyte composition.) For the purpose of this study, the reduction in thickness at 3 min elapsed time was taken as the measure of deformation. The deformation data for separator pellets based on the

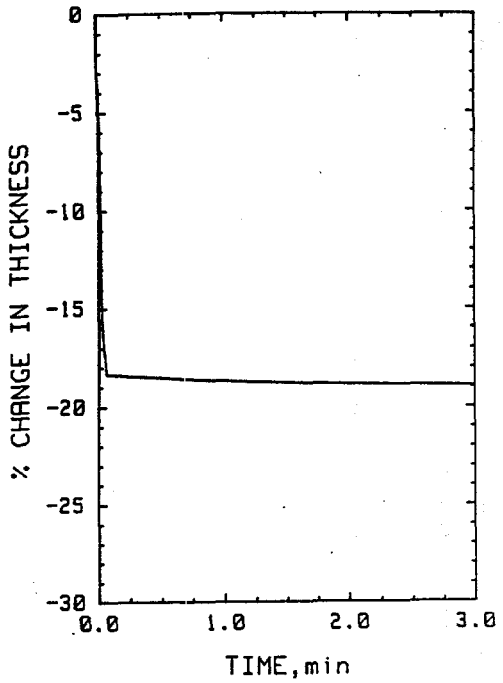

Figure 2. Representative Deformation Profile at 530°C and 14.3 Psig Applied Pressure of Separator Pellet Based on LiCl-KCl Eutectic and 35% MgO)

LiCl-KCl eutectic are summarized in Appendix A-1. [Several tests were conducted at 28.2 psig (194 kPa) applied pressure to better define the system curvature and to enable modeling for this EB composition.]

Modeling. The mean values and standard deviations for separator pellet deformation were analyzed by a least-squares regression analysis. The polynomial coefficients (parameter estimates) for the EB mix based on LiCl-KCl eutectic and 35% MgO are listed in Appendix B-1. Appendix C-1 lists the percentage reduction in thickness (deformation) predicted by the model and the corresponding measured values for the various experimental conditions. The estimated values of deformation were calculated from:

$$Y = 100[(e^z/(1+e^z)] \qquad [5]$$

where z is the logit-model expression evaluated at the appropriate values of P^*, T^*, and D^*, with parameter estimates (e.g., b_0) substituted for the corresponding model parameter. For the EB with LiCl-KCl eutectic and 35% MgO, the expression for z is:

$$z = b_0 + b_1P^* + b_3D^* + b_{13}P^*D^* + b_{11}P^{*2}$$

$$+ b_{33}D^{*2} + \gamma P^{*2}D^{*2} \qquad [6]$$

For example, at 80% TD and an applied pressure of 23.8 psig, D^* and P^* are 0.280 and 0.90, respectively. Using these values in Eq. 6, z is calculated to be 0.106 and, using Eq. 5, Y is found to be 52.6%. The values of Y in Appendix C-1 were determined in this way.

The fraction of the variation of the logit-transformed response about the mean value that is explained by the model can be summarized by the squared correlation coefficient, R^2. In this case, $R^2 = 0.93$. Thus, 93% of the variation of the response was explained by the model.

The estimated response surfaces (contour plots) for deformation are shown in Figure 3 as a function of % TD and applied pressure for temperatures of 500° to 560°C. (Because of the lack of temperature dependence, only a single graph is presented.)

The arrow on the figure refers to the nominal value called out for the density of separator pellets for Li(Si)/FeS_2 thermal batteries designed at SNL. The data of Figure 3 indicate that the design point should be moved to 73.4% TD, to minimize the effect of applied pressure on pellet deformation.

Empirically, the amount of separator pellet deformation that is acceptable for battery purposes lies within the range of ~15% to

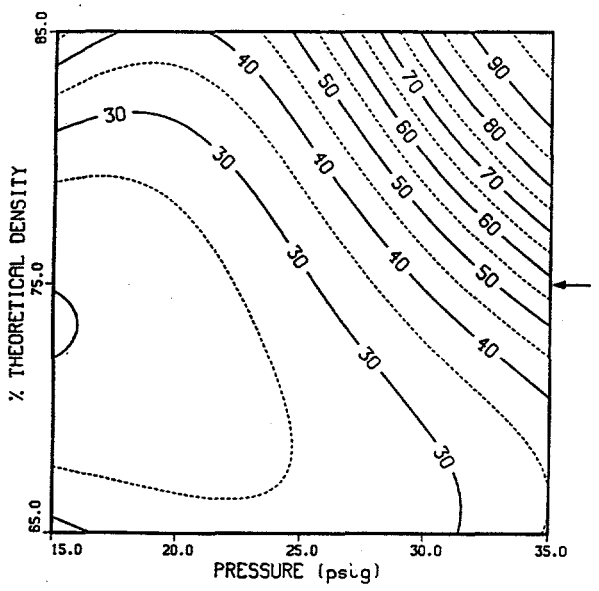

Figure 3. Contour Plot for Estimated Deformation of EB Pellets Based on LiCl-KCl Eutectic and 35% MgO as a Function of Applied Pressure and % Theoretical Density for Temperature of 500°C to 560°C

30%. Separator pellets with deformation higher than this will still work, but at the risk of reduced battery reliability if excessive electrolyte leakage into the battery insulation (wrap) occurs. Separator pellets with values lower than this range can experience reduced wetting of the adjacent anode and cathode pellets. The reduction in wetting can then increase the impedance of the cell, which can adversely impact performance.

Under a stack pressure of 15 psig, the deformation of separator pellets will be ~20%, which is acceptable. (It should be emphasized here that the stack pressure refers to the pressure on the stack after the battery has been activated and does not represent the closing pressure, which is typically >175 psig.) However, once a stack pressure of ~26 psig is exceeded, deformation will be greater than 30%. Under these conditions, potential problems could arise in a thermal battery during discharge, due to excessive separator pellet deformation.

The predicted deformation of separator pellets with 35% MgO at an applied pressure of 15 psig and 35 psig is shown in Table 4 at the design point of 75% TD.

The deformation at an applied pressure of 35 psig is excessive; this could lead to problems during discharge for a thermal battery using such a material for the separator if the stack pressure is sustained at this level.

Thus, if information is available for the critical parameters (namely, applied pressure, % TD, and temperature) during discharge of a thermal battery, such contour maps are valuable from a thermal-battery design perspective. Because pellets are pressed to a specific density, the % TD will already be known. Stack pressure can be recorded by incorporating a load cell into a battery. [Such tests have already been conducted at SNL and will be the subject of a separate report.[8]] Stack temperatures can be recorded by insertion of a thin, flattened thermocouple into the battery stack during construction. Care must be taken, however, to avoid possible shorting of cells–especially with thin cells, where pellet thickness can be as low as 0.020 cm (0.008 in).

LiCl-KCl (Standard) Electrolyte: 40% MgO

Modeling. The polynomial coefficients for the deformation model for the EB with 40% MgO are listed in Appendix B-2. The percentage reduction in thickness estimated by the model is listed in Appendix C-2, with the corresponding measured values for the range of experimental conditions. Note that this EB composition uses the simplest model for deformation of all the mixes examined in this

Table 4. Deformation of Separator Pellets Based on LiCl-KCl Eutectic and 35% MgO at 75% TD*

Temperature, °C	Pressure, psig	% Reduction in Thickness
500-560	15	20.1
500-560	35	58.2

* Predicted using the model shown Appendix B-1.

study. It includes only terms for % TD and applied pressure and has no interaction terms (see Table 3).

One area where poor agreement was observed between predicted and measured values of deformation is at the highest pressure and % TD. Deformation between 55% and 60% was measured, while the model predicts only 13%. The squared correlation coefficient (R^2) was 0.97. Thus, 97% of the variation of the logit-transformed response was explained by the model. (The high-pressure, high-% TD deformation data were not included in the regression analysis or computation of R^2.)

The estimated response surface for deformation is shown in Figure 4 as a function of % TD and applied pressure for temperatures of 500°C to 560°C. (The upper right-hand corner of the contour plot is blanked out because of the poor agreement of the model with the experimental data in this region.) The predicted deformation of separator pellets with 40% MgO at an applied pressure of 15 psig and 35 psig is shown in Table 5 at the design point of 75% TD.

The deformation is well within the acceptable response for the entire pressure region.

In comparison, the deformation for the comparable EB with 35% MgO while acceptable at 15 psig (20.1%) was high for the highest pressure (58.2%) (Table 4). Thus, the deformation of separator pellets of LiCl-KCl eutectic with 40% MgO is much more "robust" to changes in applied pressure and % TD. The specified design point of 75% TD appears acceptable for this EB composition.

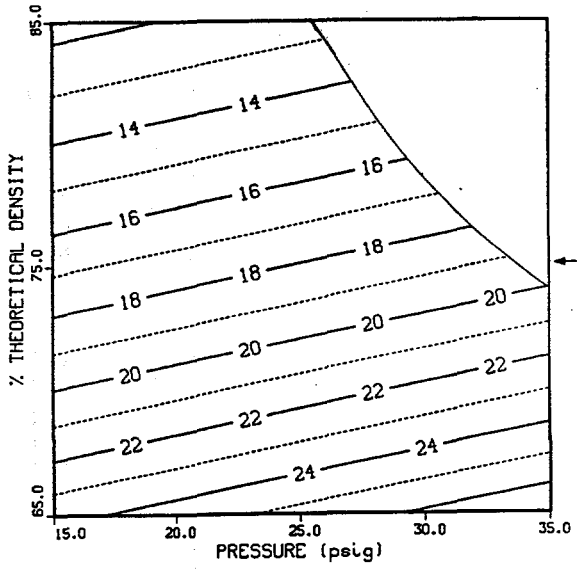

Figure 4. Contour Plot for Estimated Deformation of EB Pellets Based on LiCl-KCl Eutectic and 40% MgO as a Function of Applied Pressure and % Theoretical Density for Temperatures of 500°C - 560°C

Table 5. Deformation of Separator Pellets Based on LiCl-KCl Eutectic and 40% MgO at 75% TD*

Temperature, °C	Pressure, psig	% Reduction in Thickness
500-560	15	16.8
500-560	35	19.4

*Predicted using the model shown in Appendix B-2.

LiCl-LiBr-KBr (LM#1) Electrolyte: 25% MgO

The deformation data for separator pellets based on the LiCl-LiBr-KBr eutectic electrolyte and 25% MgO are summarized in Appendix A-2

Modeling. The polynomial coefficients for the deformation model for the LM#1 EB with 25% MgO are listed in Appendix B-3. The percentage reduction in thickness predicted by the model is listed in Appendix C-3, with the corresponding measured values for the various experimental conditions.

Note that the model for this EB mix includes temperature, pressure, and density terms as well as a squared term (D) and an interaction term (PD). In this case, R^2 was 0.98.

The estimated response surfaces for deformation are shown in Figures 5a and 5b as a function of % TD and applied pressure for temperatures of 500°C and 560°C, respectively. The predicted deformation of separator pellets with 25% MgO at applied pressures of 15 psig and 35 psig is shown in Table 6 at the design point of 75% TD for temperatures of 500°C and 560°C.

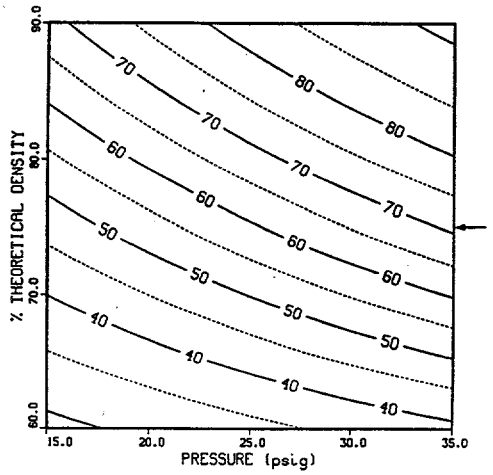

Figure 5A. Contour Plot for Estimated Deformation of EB Pellets Based on LiCl- LiBr-KBr Eutectic and 25% MgO as a Function of Applied Pressure and % Theoretical Density for 500°C

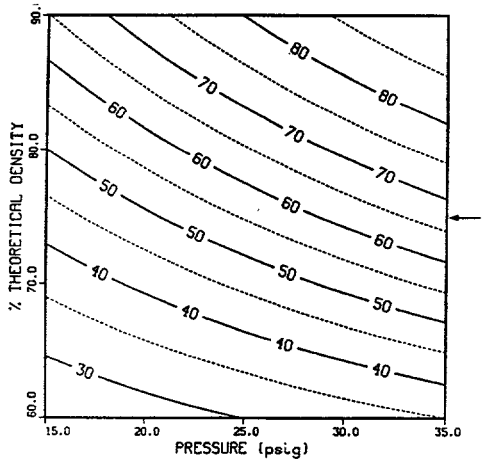

Figure 5B. Contour Plot for Estimated Deformation of EB Pellets Based on LiCl-LiBr-KBr Eutectic and 25% MgO as a Function of Applied Pressure and % Theoretical Density for 560°C

Table 6. Deformation of Separator Pellets Based on LiCl-LiBr-KBr Eutectic and 25% MgO at 75% TD*

Temperature, °C	Pressure, psig	% Reduction in Thickness
500	15	46.8
500	35	70.8
560	15	42.8
560	35	67.3

*Predicted using the model shown in Appendix B-3

Pellet deformation was excessive (>30%) in all cases. As a result, this EB composition would not be acceptable for use in separator pellets in thermal batteries at the design point of 75% TD. Lowering the pellet density to 60% TD would not solve the problem

LiCl-LiBr-KBr (LM#1) Electrolyte: 30% MgO

The deformation data for separator pellets based on the LiCl-LiBr-KBr eutectic electrolyte and 30% MgO are summarized in Appendix C-2. Increasing the binder content from 25% to 30% reduced the separator-pellet deformation considerably.

Modeling. The polynomial coefficients for the deformation model for the LM#1 electrolyte with 30% MgO are listed in Appendix B-4. The model for this EB composition is the same as for the EB with 25% MgO. The percent reduction in thickness predicted by the model is listed in Appendix C-3 with the corresponding measured values for the various experimental conditions (R^2=0.96).

The estimated response surfaces for pellet deformation are shown in Figures 6a and 6b for temperatures of 500°C and 560°C, respectively. The wide contours between 60% and 85% TD are highly desirable because this indicates that deformation is relatively insensitive to large changes in applied pressures and % TD. The estimated deformation of separator pellets with 30% MgO at applied pressures of 15 psig and 35 psig is shown in Table 7 at the pellet-density design point of 75% TD for temperatures of 500°C and 560°C.

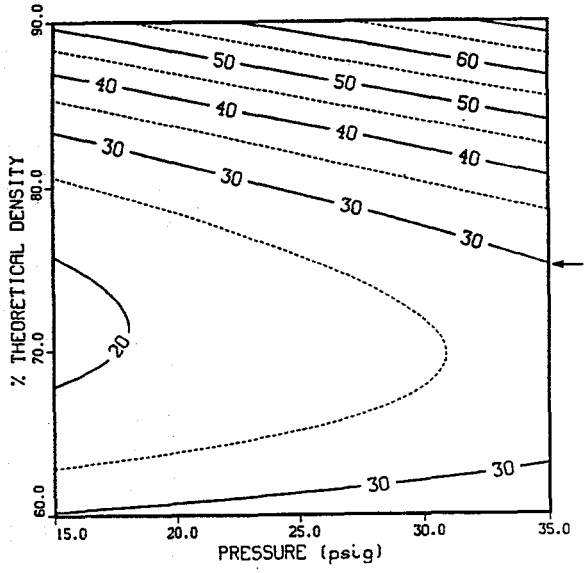

Figure 6A. Contour Plot for Estimated Deformation of EB Pellets Based on LiCl-LiBr-KBr Eutectic and 30% MgO as a Function of Applied Pressure and % Theoretical Density for 500°C.

Table 7. Deformation of Separator Pellets Based on LiCl-LiBr-KBr Eutectic and 30% MgO at 75% TD*

Temperature, °C	Pressure, psig	% Reduction in Thickness
500	15	19.6
500	35	29.9
560	15	18.1
560	35	27.8

*Predicted using the model shown in Appendix B-3

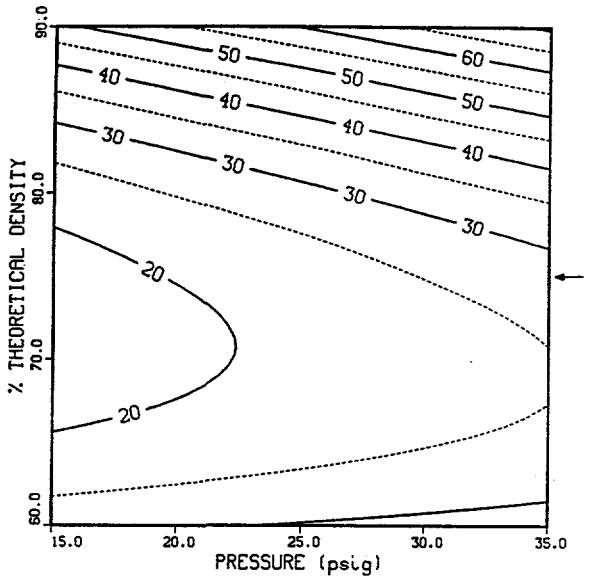

Figure 6B. Contour Plot for Estimated Deformation of EB Pellets Based on LiCl-LiBr-KBr Eutectic and 30% MgO as a Function of Applied Pressure and % Theoretical Density for 560°C.

In all cases, the deformation lies within the acceptable region of 15% to 30%. This EB composition is thus considered robust with respect to deformation over the full range of experimental conditions tested and would be a suitable candidate for use as a separator in thermal batteries. This robustness would be further enhanced if the pellet-density design point were reduced slightly from 75% to about 70% TD.

LiBr-KBr-LiF (LM#2) Electrolyte: 25% MgO

The deformation data for separator pellets based on the LiBr-KBr-LiF eutectic electrolyte and 25% MgO are summarized in Appendix A-3.

Modeling. The polynomial coefficients for the deformation model for the LM#2 EB with 25% MgO are listed in Appendix B-5. The percentage reduction in thickness predicted by the model is listed in Appendix C-5, with the corresponding measured values for the various experimental conditions. The model for this EB mix is identical to that for the LM#1 EB mixes (R^2=0.98).

The estimated response surfaces for pellet deformation are shown in Figures 7a and 7b as a function of % TD and applied pressure for temperatures of 500°C and 560°C, respectively. The estimated deformation of separator pellets with 25% MgO at applied pressures of 15 psig and 35 psig is listed in Table 8 at the pellet-density design point of 75% TD for temperatures of 500°C and 560°C.

Table 8. Deformation of Separator Pellets Based Upon LiBr-KBr-LiF Eutectic and 25% MgO at 75% TD*

Temperature, °C	Pressure, psig	% Reduction in Thickness
500	15	13.8
500	35	25.4
560	15	12.4
560	35	23.2

* Predicted using the model shown in Appendix B-5

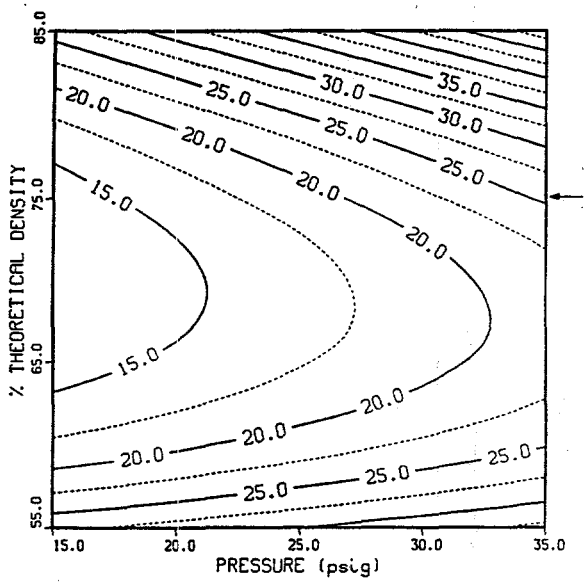

Figure 7A. Contour Plot for Estimated Deformation of EB Pellets Based on LiBr-KBr-LiF Eutectic and 25% MgO as a Function of Applied Pressure and % Theoretical Density for 500°C

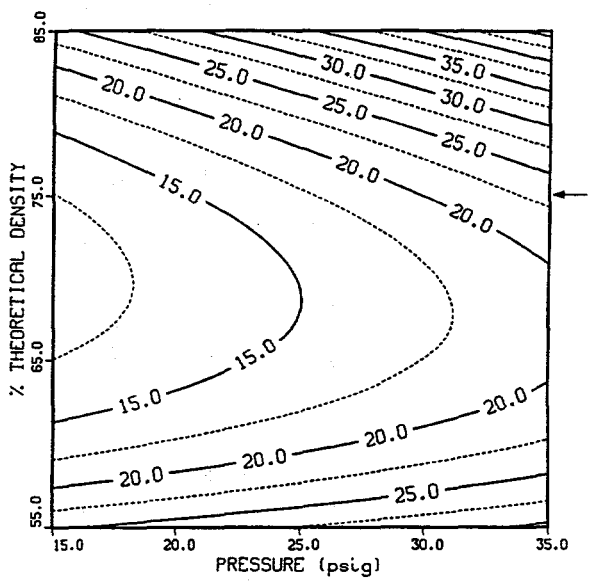

Figure 7B. Contour Plot for Estimated Deformat ı of EB Pellets Based on LiBr-KBr-LiF Eutectic and 25% MgO as a Function of Applied Pressure and % Theoretical Density for 560°C

Pellet deformation was acceptable at the higher applied pressures and was only slightly below the nominal 15% deformation limit considered acceptable. Overall, this EB composition would be considered acceptable for use in separator pellets in thermal batteries.

The robustness of this EB composition to deformation would be enhanced if the pellet-density design point were reduced from 75% to about 70% TD.

LiBr-KBr-LiF (LM#2) Electrolyte: 30% MgO

The deformation data for separator pellets based on the LiBr-KBr-LiF eutectic electrolyte and 30% MgO are summarized in Appendix A-5. Increasing the binder content from 25% to 30% caused a large reduction in pellet deformation—especially at the higher pellet densities.

Modeling. The polynomial coefficients for the deformation model for the LM#2 EB with 30% MgO are listed in Appendix B-6. The percentage reduction in thickness predicted by the model is listed in Appendix C-6, with the corresponding measured values for the various experimental conditions. The model for this EB is identical to that for the LM#2 EB with 25% MgO (R^2=0.92).

The estimated response surfaces for pellet deformation are shown in Figures 8a and 8b for temperatures of 500°C and 560°C, respectively. The estimated deformation of separator pellets with 30% MgO is listed in Table 9 at the pellet-density design point of 75% TD for temperatures of 500°C and 560°C.

Increasing the binder content of the LM#2 EB from 25% to 30% MgO caused a large reduction in deformation at the pellet-density design point of 75% TD. In all cases, the deformation was less than the lower limit of 15% considered acceptable for thermal-battery use. The data for the LM#2 EB with 25% MgO (Table 6) show this material to be preferred over the counterpart with 30% MgO (Table 7).

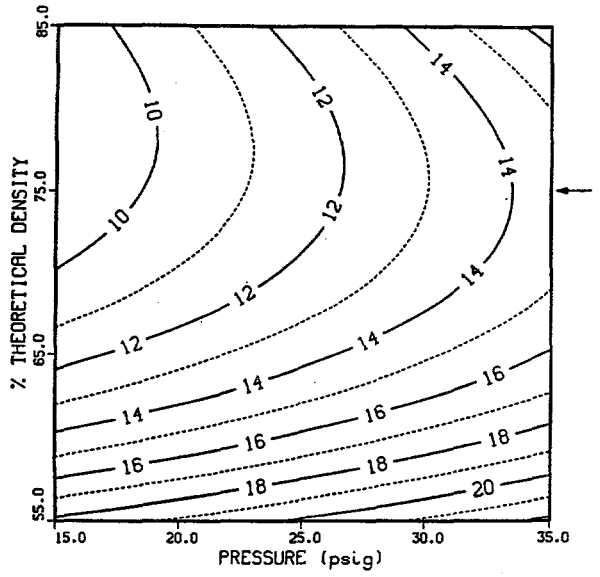

Figure 8A. Contour Plot for Estimated Deformation of EB Pellets Based on Li-Br-KBr-LiF Eutectic and 30% MgO as a Function of Applied Pressure and % Theoretical Density for 500°C

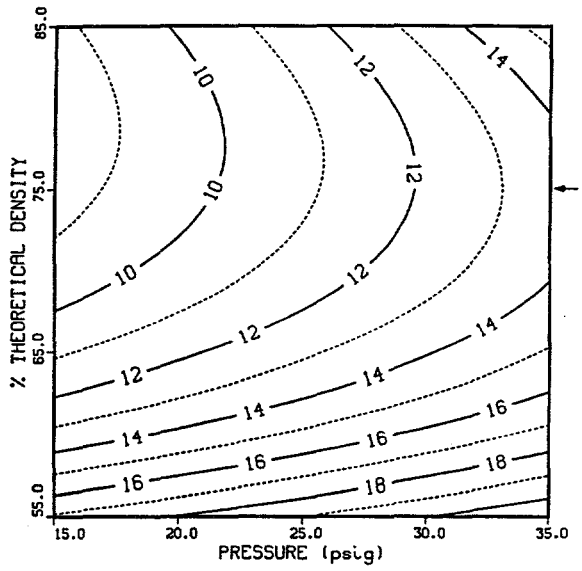

Figure 8B Contour Plot for Estimated Deformation of EB Pellets Based on Li-Br-KBr-LiF Eutectic and 30% MgO as a Function of Applied Pressure and % Theoretical Density for 560°C

Table 9. Deformation of Separator Pellets Based on LiBr-KBr-LiF Eutectic and 30% MgO at 75% TD*

Temperature, °C	Pressure, psig	% Reduction in Thickness
500	15	9.2
500	35	14.5
560	15	8.6
560	35	13.6

* Predicted using the model shown in Appendix B-5

LiCl-LiBr-LiF (All-Li) Electrolyte: 30% MgO

The deformation data for separator pellets based on the LiCl-LiBr-LiF minimum-melting electrolyte and 30% MgO are summarized in Appendix A-4.

Modeling. The polynomial coefficients for the deformation model for the all-Li EB with 30% MgO are listed in Appendix B-7. The percentage reduction in thickness predicted by the model is listed in Appendix C-7, with the corresponding measured values for the various experimental conditions. The model is similar to those for the LM#1 and LM#2 EBs, except that it also includes a P-squared term (R^2 =0.98).

The estimated response surfaces for pellet deformation are shown in Figures 9a and 9b for temperatures of 500°C and 560°C, respectively. The estimated deformation of separator pellets at applied pressures of 15 psig and 35 psig is listed in Table 10 at the pellet-density design point of 75% TD for temperatures of 500°C and 560°C.

Reducing the pellet-density design point from 75% TD to the optimum value of 70.5% TD would center the contour lines between 15 psig and 35 psig. However, the pellet deformation would still be >30% for all conditions, which makes this EB composition unacceptable for use in separator pellets in thermal batteries.

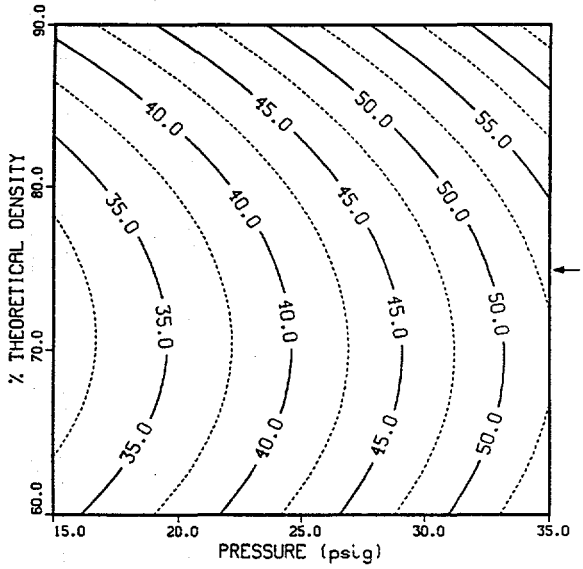

Figure 9A. Contour Plot for Estimated Deformation of EB Pellets Based on LiCl-LiBr-LiF Electrolyte and 30% MgO as a Function of Applied Pressure and % Theoretical Density for 500°C

Table 10. Deformation of Separator Pellets Based on LiCl-LiBr-LiF Electrolyte and 30% MgO at 75% TD*

Temperature, °C	Pressure, psig	% Reduction in Thickness
500	15	35.3
500	35	64.4
560	15	32.3
560	35	61.2

*Predicted using the model shown in Appendix B-7

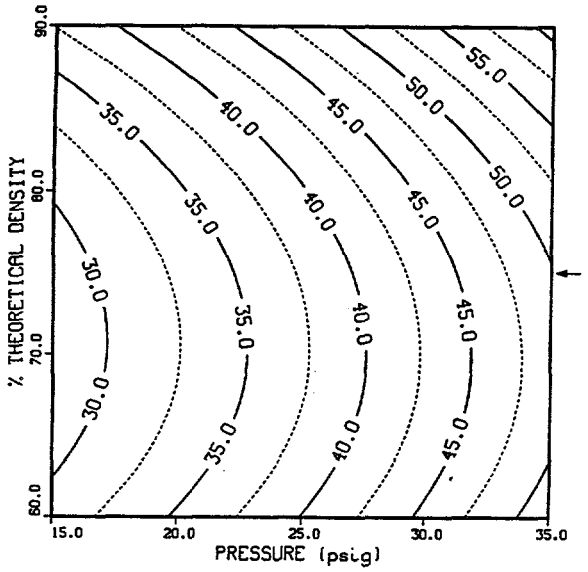

Figure 9B. Contour Plot for Estimated Deformation of EB Pellets Based on LiCl-LiBr-LiF Electrolyte and 30% MgO as a Function of Applied Pressure and % Theoretical Density for 560°C

LiCl-LiBr-LiF (All-Li) Electrolyte: 35% MgO

The deformation data for separator pellets based on the LiCl-LiBr-LiF minimum-melting electrolyte and 35% MgO are summarized in Appendix A-4. As expected, increasing the binder content from 30% to 35% resulted in a large reduction in the pellet deformation.

Modeling. The polynomial coefficients for the deformation model for the all-Li EB with 35% MgO are listed in Appendix B-8. The percentage reduction in thickness predicted by the model is listed in Appendix C-8, with the corresponding measured values for the various experimental conditions. The model form is identical to that for the all-Li EB with 30% MgO (R^2=0.98).

The estimated response surfaces for pellet deformation are shown in Figures 10a and 10b for temperatures of 500°C and 560°C, respectively. The estimated deformation of separator pellets at applied pressures of 15 psig and 35 psig is listed in Table 11 at the pellet-density design point of 75% TD for temperatures of 500°C and 560°C.

Table 11. Deformation of Separator Pellets Based on LiCl-LiBr-LiF Electrolyte and 35% MgO at 75% TD*

Temperature, °C	Pressure, psig	% Reduction in Thickness
500	15	17.4
500	35	41.4
560	15	15.9
560	35	38.9

*Estimated using the model shown in Appendix B-7

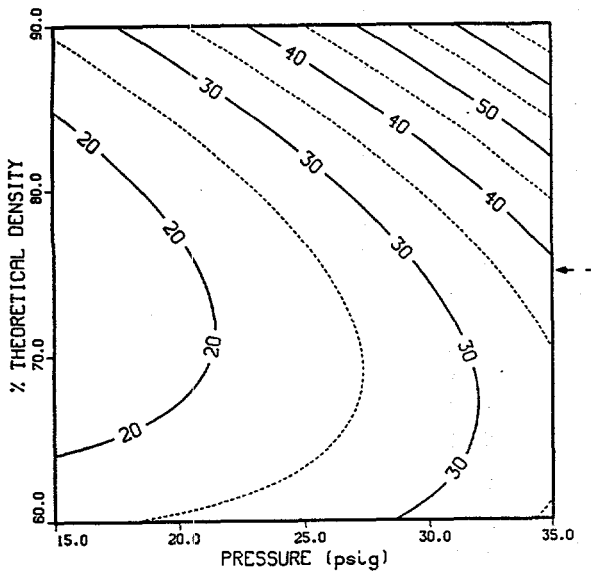

Figure 10A. Contour Plot for Estimated Deformation of EB Pellets Based on LiCl-LiBr-LiF Electrolyte and 35% MgO as a Function of Applied Pressure and % Theoretical Density for 500°C

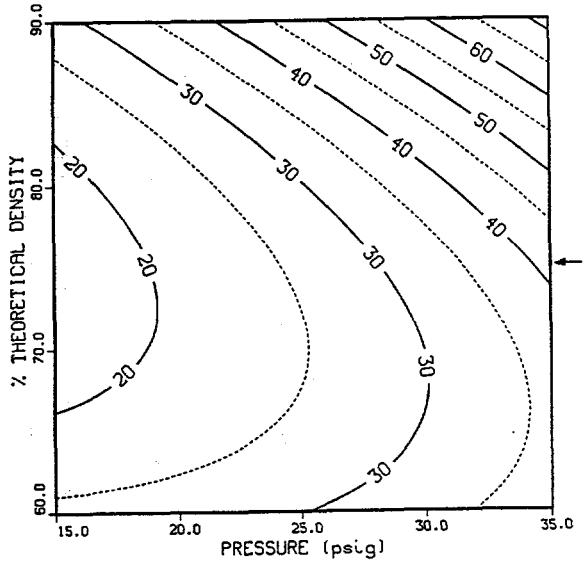

Figure 10B. Contour Plot for Estimated Deformation of EB Pellets Based on LiCl-LiBr-LiF Electrolyte and 35% MgO as a Function of Applied Pressure and % Theoretical Density for 560°C

At the lower pressure, pellet deformation is in the acceptable range. At the higher pressure, however, the deformation is greater than the desired maximum of 30%. The data of Figures 10a and 10b show that the contour lines are substantially skewed to lower % TDs as the pressure is increased. This has the effect of making the separator pellet more sensitive to applied pressure for a given % TD. The optimum pellet-density design point of ~74.1% TD at 15 psig is shifted to ~64.3% TD at 35% psig. These data suggest that the design point should be reduced from 75% to ~ 70% TD. This will reduce the maximum deformation and bring the value closer to the desired value of 30%.

At 75% TD, the deformation will reach 30% at pressures of 28.0 psig and 30 psig at 500 °C and 560°C, respectively. In comparison, at the optimum value of 69.2% TD, these values are predicted to ~ 30.0 psig and 31.9 psig—about 2 psig higher.

For critical thermal-battery application, an EB composition higher in binder than 35% MgO (e.g., 40%) may be necessary to avoid excessive separator pellet deformation.

Discussion

Because of the number of possibilities that arise during the deformation process, the resulting deformation curve can be considerably different under different experimental conditions. While only the change in thickness was monitored during the deformation process, a change in the area of the pellet could also occur due to radial movement.

Density Effects

The change in deformation with increase in the level of density shows several trends. In the first case (Type A), the deformation increases with an increase in % TD. We attribute this to an initial collapse of the primary pore structure followed by gradual radial movement of the EB material with accompanying decrease in pellet thickness. This behavior is shown by the standard EB with 35% MgO and the LM#1 EB with 25% MgO for all temperatures and pressures.

In the second case (Type B), the deformation exhibits a minimum with increase in % TD. At the lowest % TD, the porosity is large, so that this material is expected to show a relatively large reduction in thickness once the electrolyte melts, with little radial movement of material. At intermediate densities, the relative change in thickness would be less. At the highest densities, however, the initial change in thickness would be even lower, but would be accompanied by an increase in the area due to plastic flow in the radial direction. The latter would be expected to dominate the deformation process under these conditions, resulting in the observed overall increase in deformation.

In the third case (Type C), the deformation shows a gradual decrease in deformation with increase in % TD. At the highest % TD, for example, the extent of radial movement is limited because of the rheology of the particular EB composition. As the porosity gradually decreases with increase in % TD, the degree of pore collapse becomes increasingly less, resulting in a gradual decrease in the observed change in thickness once the electrolyte melts. However, if the system experiences significant radial movement at the higher densities as a result of plastic flow, the deformation will increase again, resulting in Type B behavior. Type C behavior is shown by the all-Li EB with 30% MgO and the LM#2 EB with 25% MgO for all temperatures and pressures.

Temperature Effects

The reduction in deformation usually observed with increase in temperature was surprising. An increase in deformation

would be expected based on the reduced viscosity and surface tension of the molten electrolyte at higher temperatures. For the LiCl-KCl eutectic, for example, the viscosity is reduced from 2.23 mNs/m^2 to 1.77 mNs/m^2 in going from 500°C to 560°C. The change in surface tension under the same conditions is 126 mN/m to 121 mN/m, respectively, not nearly as large.[9]

The temperature effect may be related to the lower actual density of the pellet at the higher temperatures caused by expansion of the molten electrolyte. This results in a smaller change in thickness during the deformation test relative to the lower temperatures, leading to a Type C curve.

Pressure Effects

The effect of pressure on the deformation process was consistent for all the EBs studied. Increasing the pressure caused an increase in the observed deformation for all temperatures and densities.

Rheology

The overall observed deformation depends on the degree of pore collapse and radial movement of the EB. The relative contribution of each process determines the final type of deformation that is observed, i.e., whether the deformation response is Type A, B, or C.

The rheology of an EB pellet under the experimental conditions of the study is very complicated and is influenced by the composition of the electrolyte as well as the MgO content. The surface tension of the electrolyte influences the wetting behavior with the MgO binder. This, in turn, dictates the amount of binder necessary for effective immobilization of the molten electrolyte at elevated temperatures. The conditions of EB processing (e.g., temperature, time, atmosphere, electrolyte purity, MgO purity, etc.) have a significant effect on the final physical properties of the resultant EB material. Changes in processing parameters are readily reflected in the deformation behavior of the pellets made from the EB mixes.

It should be emphasized that the deformation process in an actual thermal-battery environment will be different from that experienced by the pellets in the present study where the pressure and temperature were held constant. During assembly, the battery stack is subjected to a high pressure (typically 150 psig to 250 psig) to maintain good interfacial contact before being sealed into a case.

Once the battery is activated, the stack pressure relaxes immediately to a low steady-state level of only 10 psig to 40 psig.[8] This relaxation process is almost entirely a result of the deformation of the separator pellet caused by the melting of the electrolyte. The temperature of the battery also changes significantly, rising on activation to some peak value and then declining until the electrolyte freezes at the end of life as a result of heat loss in the battery. Since the battery stack is tightly wrapped with glass tape and insulating ceramic blankets, the tendency for radial movement of separator material will be drastically reduced relative to an unconfined pellet.

In addition, there is always a tendency for the electrolyte to wick into the insulating wrap. This is a competition between the MgO and the wrap for the molten electrolyte. Because the electrolyte is already wicked into the pores of the MgO, the tendency for de-wetting is normally minimal and only becomes a problem if the battery overheats.

Given such dynamic battery conditions, it would be very difficult to predict accurately

the extent of pellet deformation in a thermal-battery environment. The extent of deformation will certainly be different in an actual battery compared to that observed with the deformation tester used in this work. However, the results of the present study are still useful for determining the relative impact of major changes in some critical parameters that influence the deformation process.

Factor Interactions

Varying the factors in a "one-at-a-time " approach would not show the interactions that were revealed in the approach used in this study. The strength of the statistically designed experiments lies in the ability to not only determine the relative importance of each factor, but to detect the presence of interactions as well (e.g., PD effects). The other advantage of statistically designed experiments is efficiency, i.e., the maximum amount of information is obtained in the least number of experiments.

The effect of the various factors on the deformation process is readily revealed in the coefficients for the various polynomial expressions that were derived from the experimental data. These could be either positive or negative. A positive sign indicates that an increase in the independent parameter caused an increase in the deformation, while a negative sign showed a reduction in the deformation. The signs of the coefficients for the terms in the polynomial expressions for the various EBs are summarized in Table 12.

The P, PD, D^2, and P^2 coefficients were positive in all cases where that applied, as were the PD coefficients. This contrasts with the T coefficients that were negative in all cases that applied. The D coefficient was either negative or positive, depending on the EB composition.

The relative magnitude of the coefficients indicates the importance of each term. The data in Appendices B-1 to B-8 show that the D^2 term is the most important in all cases but one, with the temperature term being the least important. The pressure term was always positive, while the sign of the density term varied. Consequently, the PD interaction term was often significant at high

Table 12. Signs of Coefficients for Variables in Polynomial Expressions for Deformation of EB Pellets

		Terms					
Electrolyte	MgO	D	P	T	PD	P^2	D^2
LiCl-KCl	35	+	+	NA*	+	+	+
LiCl-KCl	40	-	+	NA	NA	NA	NA
LiCl-LiBr-KBr	25	+	+	-	+	NA	+
LiCl-LiBr-KBr	30	-	+	-	+	NA	+
LiBr-KBr-LiF	25	+	+	-	+	NA	+
LiBr-KBr-LiF	30	-	+	-	+	NA	+
LiCl-LiBr-LiF	30	-	+	-	+	+	+
LiCl-LiBr-LiF	35	-	+	-	+	+	+

Note: NA = not applicable.

positive densities, since this inhanced the pressure effect. These key points would not have been evident with the standard "one-at-a-time" approach to studying the contributions of each experimental factor.

Experimental Limitations

The data generated in the present work apply for only relatively thick pellets—nominally 1.5 mm (0.059") thick. It is unknown if the same trends would hold true with separators that are used in so-called thin-cell batteries, since these separators are only 0.008 inch to 0.010 inch thick. It would be very difficult to conduct deformation tests with pellets this thin, since the absolute magnitude of the change in thickness would be very small. The tests would result in a large experimental error that would make it difficult to statistically determine the relative impact of changes in the experimental factors on the measured pellet deformation.

A deformation of 2% corresponds to a vertical displacement of 0.0011" (0.078 mm). A displacement of 0.001" (1 mil) is easily measured with good precision using 1.5-mm-thick pellets. However, for a 0.010 in-thick pellet, the same amount of deformation would result in a vertical displacement of only 0.0002" (0.2 mils). Such a low value could not be measured accurately with the present experimental setup. In addition, the effect of parallelism of the pellet faces becomes increasingly important.

The present data do not address the issue of radial movement of material during the deformation process. The present technique measures only vertical (axial) displacement of the pellet. The areal changes in the pellets would need to be measured as well to shed more light on the rheology of molten EB pellets under a wide range of experimental conditions. This would not be straightforward, since the pellets do not always grow uniformly in the radial direction. The asymmetric growth would necessitate using some type of sophisticated areal-measurement technique (e.g., digitizing the outline of the pellet and calculating the area of the resulting shape).

Optimum EB Densities and Battery-Design Implications

The optimum conditions for pressing separator pellets to minimize excessive deformation can readily be determined by studying the contour plots and the associated regression models. The optimum densities for the various EB compositions as determined from the contour plots are summarized in Table 13 for comparison to the current design value of 75% TD. The EB compositions that are suitable for use as separators in thermal batteries are marked in Table 13 with an asterisk. These density values are the ones the thermal-battery engineer should use for prototype battery development. Only the EBs based on LiCl-KCl eutectic and the LM#2 EB with 30% MgO have predicted optimum densities that are very close to the current design value of 75% TD.

There is a tradeoff between electrochemical performance and the mechanical properties of the EB pellets when used as separators in thermal batteries. Increasing the MgO content of the EBs to reduce the deformation will cause a concomitant increase in the resistivity.[10]

This could impact the pulse performance of the battery under a heavy load. The thermal-battery engineer will have to address this tradeoff for each particular application. This becomes most important when the battery is to be subjected to a severe environment (e.g., high levels of shock, acceleration, vibration, or spin).

Table 13. Optimum Densities for Various EBs Examined in This Work

Electrolyte	Optimum % MgO	% Theoretical Density	Density g/cc#
LiCl-KCl Eutectic	35*	73.4	1.75
LiCl-KCl Eutectic	40*	76.0	1.84
LiCl-LiBr-KBr Eutectic	25	NA	NA
LiCl-LiBr-KBr Eutectic	30*	69.3	2.11
LiBr-KBr-LiF Eutectic	25*	68.6	2.35
LiBr-KBr-LiF Eutectic	30*	76.1	2.46
LiCl-LiBr-LiF Electrolyte	30	70.5	2.19
LiCl-LiBr-LiF Electrolyte	35*	69.2	2.17

Tolerance of ± 0.05 g/cc
* Composition suitable for use as separator in thermal battery

Conclusions

The effects of factors such as pellet density, temperature, and applied pressure were statistically examined for their impact on the deformation of EB pellets for four electrolytes with two levels of MgO binder. The deformation study was conducted using a statistical design-of-experiment approach that allows the effect of a relatively large number of factors to be studied with a minimal number of experiments. This approach allows the impact of each factor to be determined and to detect the presence of interactions, as well. Contour plots of the estimated response surfaces were generated over the range of experimental conditions examined in the study for purposes of interpretation.

All compositions except the LiCl-LiBr-KBr (LM#1) eutectic with 25% MgO and the LiCl-LiBr-LiF (all-Li) electrolyte with 30% MgO are suitable for use as separators in thermal batteries. The study has provided estimates of the optimum densities for each of the EBs studied (Table 13). Generally (except for the all-Li mix), the variation in density dominated the deformation behavior across the various compositions. Changes in pressure also resulted in significant changes in deformation behavior; the specific effect of pressure depended on the level of pressure. Over the conditions studied, temperature seemed to have only minor effects.

The rheology of the molten EB pellets is very complex and is influenced strongly by the composition of the electrolyte and level of MgO binder. Three types of deformation behavior were found in the study with increase in pellet density:

- an increase in deformation (Type A curve)
- a minimum in deformation (Type B curve)
- a decrease in deformation (Type C curve).

The relative behavior of the EB (type of deformation curve) is influenced by the relative contribution of pore collapse and radial movement of the EB during the deformation process.

The impact on the conductivity of the EB mix must be considered when increasing the MgO content of the EB to improve its mechanical properties when used as a separator in thermal batteries. In general, a tradeoff must be made between these two important parameters by the thermal-battery design engineer

References

1. R. A. Guidotti and F. W. Reinhardt, "Characterization of Electrolyte-Binder Mixes for Use in Thermal Batteries," *SAND90-2103* (Albuquerque, NM: Sandia National Laboratories,) March 1991.

2. N. N. Volkov and L. A. Dubinskaya, "Ternary Reciprocal System of Lithium and Potassium Fluorides and Bromides," *Izvestiya Fiziko-khimicheskogo Nauchno-issledovatel'skogo instituta pri Irkutskom Gosudarstvennom universitete*, 2 (1), pp. 45-47 (1953).

3. R. A. Guidotti and L. Redey, to be published.

4. D. A. Nissen, "Processing Effects on Powders for Thermal Batteries," *SAND80-8024* (Albuquerque, NM: Sandia National Laboratories), May 1980.

5. R. A. Guidotti and F. W. Reinhardt, "Characterization of DEB Powders and Pellets for Ca/$CaCrO_4$ Thermal Batteries," *SAND83-2270* (Albuquerque, NM: Sandia National Laboratories, July 1985).

6. R. A. Guidotti and F. W. Reinhardt, "Evaluation of Alternate Electrolytes for Use in Li(Si)/FeS_2 Thermal Batteries," *Proc. of 33rd Intern. Power Sources Symposium*, pp. 369-376 (1988).

7. SAS Institute, Inc., SAS/STAT Users Guide®, Cary, NC, 1989.

8. DISSPLA, Integrated Software Systems Corp., 10505 Sorento Valley Road, San Diego, CA 92121-1698 (1981).

9. R. A. Guidotti and F. W. Reinhardt, "Stack-Relaxation Studies with Li(Si)/FeS_2 Thermal Batteries," to be published.

10. NIST Standard Reference Database 27, "NIST Properties of Molten Salts. Single Salts and Salt Mixtures Data. Density, Viscosity, Electrical Conductance, and Surface Tension," Ver. 2, National Institute of Standards and Technology, Gaithersburg, MD.

11. L. Redey, M. McParland, and R.A. Guidotti, "Resistivity Measurements of Halide/MgO Separators for Thermal Cells," *Proc. of 34th Intern. Power Sources Symposium*, pp. 128-131 (1990).

Appendix A.
Deformation of EB Pellets

Appendix A-1. Deformation of EB Pellets Based on LiCl-KCl Eutectic

Electrolyte	% MgO	Density, g/cc	% Theor. Density	% Change in Thickness @ 14.4 psig Avg.	@ 14.4 psig Std. Dev.	@ 23.8 psig Avg.	@ 23.8 psig Std. Dev.	@ 32.8 psig Avg.	@ 32.8 psig Std. Dev.	Temp., deg. C
LiCl-KCl Eut.	35	1.60	67.2	-25.5	0.8	-27.3	0.9	-29.4	0.2	500
" "	"	1.80*	75.6	-22.3	0.8	-25.2	1.6	-59.7	3.4	"
" "	"	2.00	84.0	-45.4	0.7	-57.2	8.7	-59.3	6.7	"
LiCl-KCl Eut.	35	1.60	67.2	-25.5	0.7	-26.2	0.2	-29.8	0.4	530
" "	"	1.80*	75.6	-21.0	0.9	-23.5	0.3	-60.0	2.4	"
" "	"	2.00	84.0	-42.1	0.7	-51.3	6.2	-61.8	3.7	"
LiCl-KCl Eut.	35	1.60	67.2	-24.6	0.8	-26.3	0.4	-33.8	0.8	560
" "	"	1.80*	75.6	-22.2	0.9	-25.8	0.5	-56.7	4.9	"
" "	"	2.00	84.0	-39.6	1.9	-54.5	6.4	-67.0	7.1	"
LiCl-KCl Eut.	40	1.60	65.3	-24.5	0.9	-24.9	0.6	-27.3	0.3	500
" "	"	1.85*	75.5	-15.3	0.8	-17.0	0.7	-20.7	1.9	"
" "	"	2.10	85.7	-10.6	1.5	-13.3	0.2	-59.8	3.0	"
LiCl-KCl Eut.	40	1.60	65.3	-23.4	0.4	-24.5	0.4	-26.7	0.1	530
" "	"	1.85*	75.5	-16.6	0.6	-17.3	0.8	-20.9	1.4	"
" "	"	2.10	85.7	-11.3	1.5	-11.3	1.5	-57.6	4.9	"
LiCl-KCl Eut.	40	1.60	65.3	-22.8	0.8	-24.6	1.4	-25.7	1.0	560
" "	"	1.85*	75.5	-16.3	1.4	-16.4	0.3	-17.3	0.3	"
" "	"	2.10	85.7	-12.5	1.0	-13.6	2.0	-54.9	0.5	"

* Design point used for thermal battery separators.

Appendix A–2. Deformation of EB Pellets Based on LiCl–LiBr–KBr Eutectic

Electrolyte	% MgO	Density, g/cc	% Theor. Density	% Change in Thickness @ 14.4 psig Avg.	@ 14.4 psig Std. Dev.	@ 23.8 psig Avg.	@ 23.8 psig Std. Dev.	@ 32.8 psig Avg.	@ 32.8 psig Std. Dev.	Temp., deg. C
LiCl–LiBr–KBr Eut.	25	1.90	63.3	-31.2	1.2	-34.7	0.7	-45.5	1.6	500
" "	"	2.30*	76.7	-46.2	1.7	-65.1	1.3	-64.2	5.1	"
" "	"	2.65	88.3	-67.9	3.4	-84.7	3.2	-91.4	1.3	"
LiCl–LiBr–KBr Eut.	25	1.90	63.3	-29.6	1.0	-37.2	1.4	-43.3	1.4	530
" "	"	2.30*	76.7	-49.6	2.0	-59.4	1.7	-67.4	1.3	"
" "	"	2.65	88.3	-64.3	3.1	-75.6	1.4	-90.1	0.6	"
LiCl–LiBr–KBr Eut.	25	1.90	63.3	-29.5	0.9	-34.6	0.5	-43.0	3.1	560
" "	"	2.30*	76.7	-45.7	1.9	-55.9	0.9	-57.9	6.6	"
" "	"	2.65	88.3	-55.6	5.4	-74.0	1.4	-86.1	2.1	"
LiCl–LiBr–KBr Eut.	30	1.90	62.5	-26.5	0.1	-26.9	0.8	-28.3	0.4	500
" "	"	2.30*	75.7	-18.4	0.6	-26.3	1.3	-36.2	4.0	"
" "	"	2.65	87.2	-39.0	1.7	-51.5	0.5	-60.7	2.1	"
LiCl–LiBr–KBr Eut.	30	1.90	62.5	-24.8	0.3	-26.9	0.2	-29.2	0.4	530
" "	"	2.30*	75.7	-16.8	0.4	-18.7	0.7	-37.0	3.1	"
" "	"	2.65	87.2	-40.7	0.7	-47.3	3.6	-56.6	2.3	"
LiCl–LiBr–KBr Eut.	30	1.90	62.5	-23.3	0.7	-26.8	0.7	-28.3	1.0	560
" "	"	2.30*	75.7	-19.0	0.4	-23.6	2.4	-38.8	2.7	"
" "	"	2.65	87.2	-33.6	2.9	-44.4	2.1	-55.8	0.9	"

* Design point used for thermal battery separators.

Appendix A-3. Deformation of EB Pellets Based on LiBr-KBr-LiF Eutectic

Electrolyte	% MgO	Density, g/cc	% Theor. Density	% Change in Thickness @ 14.4 psig Avg.	@ 14.4 psig Std. Dev.	@ 23.8 psig Avg.	@ 23.8 psig Std. Dev.	@ 32.8 psig Avg.	@ 32.8 psig Std. Dev.	Temp., deg. C
LiBr-KBr-LiF Eut.	25	1.90	55.6	-24.7	0.3	-27.5	0.7	-31.0	0.7	500
" "	"	2.59*	75.7	-14.4	0.3	-18.2	2.4	-25.8	1.0	"
" "	"	2.98	87.1	-31.3	1.9	-45.7	6.4	-60.8	10.6	"
LiBr-KBr-LiF Eut.	25	1.90	55.6	-24.3	0.6	-27.0	0.4	-30.1	0.3	530
" "	"	2.59*	75.7	-13.2	2.0	-17.2	1.0	-22.2	1.8	"
" "	"	2.98	87.1	-30.3	1.7	-40.9	3.6	-55.6	6.4	"
LiBr-KBr-LiF Eut.	25	1.90	55.6	-23.9	0.3	-26.2	0.3	-28.6	0.8	560
" "	"	2.59*	75.7	-13.8	1.3	-15.7	0.8	-22.0	1.8	"
" "	"	2.98	87.1	-27.9	1.6	-41.6	2.4	-45.8	5.0	"
LiBr-KBr-LiF Eut.	30	1.90	55.4	-18.0	0.4	-19.5	0.3	-21.2	0.7	500
" "	"	2.59*	75.5	-11.4	1.4	-10.9	0.2	-12.5	1.1	"
" "	"	2.90	84.5	-8.9	1.6	-10.0	1.1	-16.0	1.9	"
LiBr-KBr-LiF Eut.	30	1.90	55.4	-17.2	0.1	-18.7	0.5	-21.0	0.2	530
" "	"	2.59*	75.5	-10.6	1.1	-11.2	1.5	-11.2	1.1	"
" "	"	2.90	84.5	-7.5	2.0	-13.6	1.9	-16.2	0.4	"
LiBr-KBr-LiF Eut.	30	1.90	55.4	-16.0	0.7	-18.0	0.7	-20.9	0.2	560
" "	"	2.59*	75.5	-8.8	1.9	-10.7	1.0	-12.6	1.4	"
" "	"	2.90	84.5	-7.5	0.2	-9.2	0.4	-16.2	1.6	"

* Design point used for thermal battery separators.

Appendix A–4. Deformation of EB Pellets Based on LiCl–LiBr–LiF Eutectic

Electrolyte	% MgO	Density, g/cc	% Theor. Density	% Change in Thickness @ 14.4 psig Avg.	@ 14.4 psig Std. Dev.	@ 23.8 psig Avg.	@ 23.8 psig Std. Dev.	@ 32.8 psig Avg.	@ 32.8 psig Std. Dev.	Temp., deg. C
LiCl–LiBr–LiF Eut.	30	1.86	60.0	-33.5	0.4	-41.3	1.4	-52.4	0.8	500
" "	"	2.34*	75.5	-29.0	0.7	-40.3	0.7	-52.4	0.7	"
" "	"	2.64	85.2	-36.8	0.6	-44.9	0.8	-55.4	0.8	"
LiCl–LiBr–LiF Eut.	30	1.86	60.0	-33.8	0.6	-40.2	0.6	-50.1	1.2	530
" "	"	2.34*	75.5	-26.7	1.4	-37.6	1.3	-51.9	1.7	"
" "	"	2.64	85.2	-36.0	1.2	-44.0	0.4	-53.8	1.2	"
LiCl–LiBr–LiF Eut.	30	1.86	60.0	-31.0	0.4	-38.8	0.9	-47.3	1.4	560
" "	"	2.34*	75.5	-24.6	1.8	-37.5	0.8	-47.1	1.8	"
" "	"	2.64	85.2	-36.1	3.9	-44.0	2.4	-52.3	1.5	"
LiCl–LiBr–LiF Eut.	35	1.80	57.5	-29.9	0.3	-32.4	0.1	-37.6	0.4	500
" "	"	2.36*	75.4	-19.5	3.9	-25.0	0.7	-39.8	2.4	"
" "	"	2.66	85.0	-21.7	1.8	-34.6	3.9	-51.1	3.3	"
LiCl–LiBr–LiF Eut.	35	1.80	57.5	-29.5	0.7	-31.7	0.6	-36.6	0.9	530
" "	"	2.36*	75.4	-16.8	1.2	-23.4	0.8	-37.6	1.7	"
" "	"	2.66	85.0	-21.3	2.1	-37.5	4.6	-48.8	4.7	"
LiCl–LiBr–LiF Eut.	35	1.80	57.5	-28.2	0.9	-31.2	1.2	-35.8	0.7	560
" "	"	2.36*	75.4	-14.7	0.7	-20.9	1.0	-36.1	0.5	"
" "	"	2.66	85.0	-23.7	5.2	-34.1	4.5	-47.5	4.2	"

* Design point used for thermal battery separators.

Appendix B.
Statistical Models for Deformation of EB Pellets

The values for P*, D*, and T* in this appendix are obtained by scaling and centering P, D, and T, respectively, as follows:

$$P^* = (P-23.8)/10 \text{ (psig)}$$

$$D^* = (D-70)/20 \text{ (\% TD)}$$

$$T^* = (T-530)/30 \ (^{o}C)$$

Appendix B-1. LiCl/KCl Eutectic (Std.) Electrolyte/35% MgO*

Model

$$\log_e \left[\frac{Y}{100 - Y} \right] = \beta_0 + \beta_1 P^* + \beta_3 D^* + \beta_{13} P^* D^* + \beta_{11} P^{*2} + \beta_{33} D^{*2} + \gamma P^{*2} D^{*2} + \varepsilon$$

$\hat{\beta}_0 = -1.124$ (0.061)

$\hat{\beta}_1 = 0.376$ (0.0421)

$\hat{\beta}_3 = 0.119$ (0.20)

$\hat{\beta}_{13} = 1.561$ (0.23)

$\hat{\beta}_{11} = 0.201$ (0.0821)

$\hat{\beta}_{33} = 1.63$ (0.821)

$\hat{\gamma} = 2.74$ (0.93)

$r^2 = 0.93$

Appendix B-2. LiCl-KCl Eutectic (Std.) Electrolyte/40% MgO

Model

$$\log_e \left[\frac{Y}{100 - Y} \right] = \beta_0 + \beta_1 P^* + \beta_3 D^* + \varepsilon$$

$\hat{\beta}_0 = -1.309$ (0.012)

$\hat{\beta}_1 = 0.0877$ (0.0016)

$\hat{\beta}_3 = -0.859$ (0.034)

$r^2 = 0.97$

* The values in parentheses are the standard errors of the parameter estimates.

Appendix B-3. LiCl-LiBr-KBr Eutectic (LM#1) Electrolyte/25% MgO

Model

$$\log_e \left[\frac{Y}{100 - Y} \right] = \beta_0 + \beta_1 P^* + \beta_2 T^* + \beta_3 D^* + \beta_{13} P^* D^* + \beta_{33} D^{*2} + \varepsilon$$

$\hat{\beta}_0 = -0.121$ (0.034) $\quad\quad$ $\hat{\beta}_3 = 1.40$ (0.074)

$\hat{\beta}_1 = 0.413$ (0.035) $\quad\quad$ $\hat{\beta}_{13} = 0.374$ (0.082)

$\hat{\beta}_2 = -0.0805$ (0.028) $\quad\quad$ $\hat{\beta}_{33} = 0.110$ (0.14)

$r^2 = 0.98$

Appendix B-4. LiCl-LiBr-KBr Eutectic (LM#1) Electrolyte/30% MgO

Model - Same as that for Appendix B-3.

$\hat{\beta}_0 = -1.303$ (0.048) $\quad\quad$ $\hat{\beta}_3 = -0.107$ (0.084)

$\hat{\beta}_1 = 0.218$ (0.033) $\quad\quad$ $\hat{\beta}_{13} = 0.243$ (0.055)

$\hat{\beta}_2 = -0.0500$ (0.028) $\quad\quad$ $\hat{\beta}_{33} = 1.82$ (0.16)

$r^2 = 0.96$

Appendix B-5. LiBr-KBr-LiF (LM#2) Eutectic Electrolyte/25% MgO

Model

$$\log_e \left[\frac{Y}{100 - Y} \right] = \beta_0 + \beta_1 P^* + \beta_2 T^* + \beta_3 D^* + \beta_{13} P^* D^* + \beta_{33} D^{*2} + \varepsilon$$

$\hat{\beta}_0 = -1.710$ (0.024) $\quad\quad$ $\hat{\beta}_3 = 0.186$ (0.018)

$\hat{\beta}_1 = 0.321$ (0.016) $\quad\quad$ $\hat{\beta}_{13} = 0.233$ (0.024)

$\hat{\beta}_2 = -0.0588$ (0.012) $\quad\quad$ $\hat{\beta}_{33} = 1.637$ (0.055)

$r^2 = 0.98$

Appendix B-6. LiBr-KBr-LiF Eutectic (LM#2) Electrolyte/30% MgO

Model - Same as that for Appendix B-5.

$\hat{\beta}_0 = -2.035$ (0.054) $\quad\quad$ $\hat{\beta}_3 = -0.395$ (0.038)

$\hat{\beta}_1 = 0.222$ (0.030) $\quad\quad$ $\hat{\beta}_{13} = 0.132$ (0.045)

$\hat{\beta}_2 = -0.0378$ (0.024) $\quad\quad$ $\hat{\beta}_{33} = 0.550$ (0.123)

$r^2 = 0.92$

Appendix B-7. LiCl-LiBr-LiF Eutectic (All-Li) Electrolyte/30% MgO

Model

$$\log_e \left[\frac{Y}{100 - Y} \right] = \beta_0 + \beta_1 P^* + \beta_2 T^* + \beta_3 D^* + \beta_{13} P^* D^* + \beta_{11} P^{*2} + \beta_{33} D^{*2} + \varepsilon$$

$\hat{\beta}_0 = -0.509$ (0.027)

$\hat{\beta}_1 = 0.434$ (0.017)

$\hat{\beta}_2 = -0.0673$ (0.016)

$\hat{\beta}_3 = -0.0130$ (0.027)

$\hat{\beta}_{13} = 0.0299$ (0.031)

$\hat{\beta}_{11} = 0.0372$ (0.030)

$\hat{\beta}_{33} = 0.465$ (0.072)

$r^2 = 0.98$

Appendix B-8. LiCl-LiBr-LiF Eutectic (All-Li) Electrolyte/35% MgO

Model - Same as that for Appendix B-7.

$\hat{\beta}_0 = -1.224$ (0.026)

$\hat{\beta}_1 = 0.471$ (0.017)

$\hat{\beta}_2 = -0.0514$ (0.013)

$\hat{\beta}_3 = -0.0603$ (0.025)

$\hat{\beta}_{13} = 0.445$ (0.029)

$\hat{\beta}_{11} = 0.0981$ (0.026)

$\hat{\beta}_{33} = 1.020$ (0.081)

$r^2 = 0.98$

Appendix C.
Comparison of Predicted and Experimental Values for the Deformation of EB Pellets

Appendix C-1. LiCl-KCl Eutectic (Std.) Electrolyte/35% MgO

Pressure	% Theor. Density	Temp.	Obs. % Change ($\bar{Y}$)	Est. % Change $\hat{Y}$	Diff. $\bar{Y}-\hat{Y}$	Std. Dev. (S)
14.4	67.2	500	25.5	26.2	-0.7	0.8
14.4	67.2	530	25.5	26.2	-0.7	0.7
14.4	67.2	560	24.6	26.2	-1.2	0.8
14.4	75.6	500	22.3	20.4	1.9	0.8
14.4	75.6	530	21.0	20.4	0.6	0.9
14.4	75.6	560	22.2	20.4	1.8	0.9
14.4	84.0	500	45.4	43.5	1.9	0.7
14.4	84.0	530	42.1	43.5	-1.4	0.7
14.4	84.0	560	39.6	43.5	-3.9	1.9
23.8	67.2	500	27.3	24.8	2.5	0.9
23.8	67.2	530	26.2	24.8	1.4	0.2
23.8	67.2	560	26.3	24.8	1.5	0.4
23.8	75.6	500	25.2	27.6	-2.4	1.6
23.8	75.6	530	23.5	27.6	-4.1	0.3
23.8	75.6	560	25.8	27.6	-1.8	0.5
23.8	84.0	500	57.2	44.0	13.2	8.7
23.8	84.0	530	51.3	44.0	7.3	6.2
23.8	84.0	560	54.5	44.0	10.5	6.4
28.2	79.8	500	51.6	49.8	1.8	4.3
28.2	79.8	530	50.6	49.8	0.8	4.0
28.2	79.8	560	48.3	49.8	-1.5	2.7
32.8	67.2	500	29.4	31.9	-2.5	0.2
32.8	67.2	530	29.8	31.9	-2.1	0.4
32.8	67.2	560	33.8	31.9	1.9	0.8
32.8	75.6	500	59.7	52.6	7.1	3.4
32.8	75.6	530	60.0	52.6	7.4	2.4
32.8	75.6	560	56.7	52.6	4.1	4.9
32.8	84.0	500	59.3	91.1	31.8	6.7
32.8	84.0	530	61.8	91.1	29.3	3.7
32.8	84.0	560	67.0	91.1	24.1	7.1

Appendix C-2. LiCl-KCl Eutectic Electrolyte/40% MgO

Pressure	% Theor. Density	Temp.	Obs. % Change ($\bar{Y}$)	Est. % Change $\hat{Y}$	Diff. $\bar{Y}-\hat{Y}$	Std. Dev. (S)
14.4	65.3	500	24.5	23.3	1.2	0.9
14.4	65.3	530	23.4	23.3	0.1	0.4
14.4	65.3	560	22.8	23.3	-0.5	0.8
14.4	75.5	500	15.3	16.4	-1.1	0.8
14.4	75.5	530	16.6	16.4	0.2	0.6
14.4	75.5	560	16.3	16.4	-0.1	1.4
14.4	85.7	500	10.6	11.2	-0.6	1.5
14.4	85.7	530	11.3	11.2	0.1	1.5
14.4	85.7	560	12.5	11.2	1.3	1.0
23.8	65.3	500	24.9	24.8	0.1	0.6
23.8	65.3	530	24.5	24.8	-0.3	0.4
23.8	65.3	560	24.6	24.8	-0.2	1.4
23.8	75.5	500	17.0	17.6	-0.6	0.7
23.8	75.5	530	17.3	17.6	-0.3	0.8
23.8	75.5	560	16.4	17.6	-1.2	0.3
23.8	85.7	500	13.3	12.1	1.2	0.2
23.8	85.7	530	11.3	12.1	-0.8	1.5
23.8	85.7	560	13.6	12.1	1.5	2.0
28.2	80.0	500	14.8	15.4	-0.6	1.4
28.2	80.0	530	14.7	15.4	-0.7	0.6
28.2	80.0	560	15.2	15.4	-0.2	0.7
32.8	65.3	500	27.3	26.3	1.0	0.3
32.8	65.3	530	26.7	26.3	0.4	0.1
32.8	65.3	560	25.7	26.3	-0.6	1.0
32.8	75.5	500	20.7	18.7	2.0	1.9
32.8	75.5	530	20.9	18.7	2.2	1.4
32.8	75.5	560	17.3	18.7	-1.4	0.3
32.8	85.7	500	59.8	13.0	46.8	3.0
32.8	85.7	530	57.6	13.0	44.6	4.9
32.8	85.7	560	54.9	13.0	41.9	0.5

Appendix C-3. LiCl-LiBr-KBr Eutectic (LM#1) Electrolyte/25% MgO

Pressure	% Theor. Density	Temp.	Obs. % Change ($\bar{Y}$)	Est. % Change $\hat{Y}$	Diff. ($\bar{Y}$-$\hat{Y}$)	Std. Dev. (S)
14.4	63.3	500	31.2	31.7	-0.5	1.2
14.4	63.3	530	29.6	30.0	-0.4	1.0
14.4	63.3	560	29.5	28.3	1.2	0.9
14.4	76.7	500	46.2	48.3	-2.1	1.7
14.4	76.7	530	49.6	46.3	3.3	2.0
14.4	76.7	560	45.7	44.3	1.4	1.9
14.4	88.3	500	67.9	65.0	2.9	3.4
14.4	88.3	530	64.3	63.2	1.1	3.1
14.4	88.3	560	55.6	61.3	-5.7	5.4
23.8	63.3	500	34.7	37.8	-3.1	0.7
23.8	63.3	530	37.2	36.0	1.2	1.4
23.8	63.3	560	34.6	34.1	0.5	0.5
23.8	76.7	500	65.1	60.8	4.3	1.3
23.8	76.7	530	59.4	58.9	0.5	1.7
23.8	76.7	560	55.9	56.9	-1.0	0.9
23.8	88.3	500	84.7	79.1	5.6	3.2
23.8	88.3	530	75.6	77.7	-2.1	1.4
23.8	88.3	560	74.0	76.3	-2.3	1.4
32.8	63.3	500	45.5	44.1	1.4	1.6
32.8	63.3	530	43.3	42.1	1.2	1.4
32.8	63.3	560	43.0	40.2	2.8	3.1
32.8	76.7	500	64.2	71.6	-7.4	5.1
32.8	76.7	530	67.4	69.9	-2.5	1.3
32.8	76.7	560	57.9	68.2	-10.3	6.6
32.8	88.3	500	91.4	88.2	3.2	1.3
32.8	88.3	530	90.1	87.3	2.8	0.6
32.8	88.3	560	86.1	86.4	-0.3	2.1

Appendix C-4. LiCl-LiBr-KBr Eutectic (LM#1) Electrolyte/30% MgO

Pressure	% Theor. Density	Temp.	Obs. % Change ($\bar{Y}$)	Est. % Change $\hat{Y}$	Diff. $\bar{Y}-\hat{Y}$	Std. Dev. (S)
14.4	62.5	500	26.5	25.4	1.1	0.1
14.4	62.5	530	24.8	24.5	0.3	0.3
14.4	62.5	560	23.3	23.6	-0.3	0.7
14.4	75.7	500	18.4	19.7	-1.3	0.6
14.4	75.7	530	16.8	18.9	-2.1	0.4
14.4	75.7	560	19.0	18.2	0.8	0.4
14.4	87.2	500	39.0	40.2	-1.2	1.7
14.4	87.2	530	40.7	39.0	1.7	0.7
14.4	87.2	560	33.6	37.8	-4.2	2.9
23.8	62.5	500	26.9	27.8	-0.9	0.8
23.8	62.5	530	26.9	26.8	0.1	0.2
23.8	62.5	560	26.8	25.8	1.0	0.7
23.8	75.7	500	26.3	24.3	2.0	1.3
23.8	75.7	530	18.7	23.4	-4.7	0.7
23.8	75.7	560	23.6	22.5	1.1	2.4
23.8	87.2	500	51.5	50.1	1.4	0.5
23.8	87.2	530	47.3	48.8	-1.5	3.6
23.8	87.2	560	44.4	47.6	-3.2	2.1
32.8	62.5	500	28.3	30.1	-1.8	0.4
32.8	62.5	530	29.2	29.1	0.1	0.4
32.8	62.5	560	28.3	28.0	0.3	1.0
32.8	75.7	500	36.2	29.4	6.8	4.0
32.8	75.7	530	37.0	28.4	8.6	3.1
32.8	75.7	560	38.8	27.4	11.4	2.7
32.8	87.2	500	60.7	59.6	1.1	2.1
32.8	87.2	530	56.6	58.4	-1.8	2.3
32.8	87.2	560	55.8	57.2	-1.4	0.9

Appendix C-5. LiBr-KBr-LiF Eutectic (LM#2) Electrolyte/25% MgO

Pressure	% Theor. Density	Temp.	Obs. % Change ($\bar{Y}$)	Est. % Change $\hat{Y}$	Diff. ($\bar{Y}-\hat{Y}$)	Std. Dev. (S)
14.4	55.6	500	24.7	25.3	-0.6	0.3
14.4	55.6	530	24.3	24.2	0.1	0.6
14.4	55.6	560	23.9	23.2	0.7	0.3
14.4	75.7	500	14.4	13.8	0.6	0.3
14.4	75.7	530	13.2	13.1	0.1	2.0
14.4	75.7	560	13.8	12.5	1.3	1.3
14.4	87.1	500	31.3	31.3	0.0	1.9
14.4	87.1	530	30.3	30.1	0.2	1.7
14.4	87.1	560	27.9	28.9	-1.0	1.6
23.8	55.6	500	27.5	28.2	-0.7	0.7
23.8	55.6	530	27.0	27.0	0.0	0.4
23.8	55.6	560	26.2	25.9	0.3	0.3
23.8	75.7	500	18.2	18.8	-0.6	2.4
23.8	75.7	530	17.2	17.9	-0.7	1.0
23.8	75.7	560	15.7	17.0	-1.3	0.8
23.8	87.1	500	45.7	42.7	3.0	6.4
23.8	87.1	530	40.9	41.2	-0.3	3.6
23.8	87.1	560	41.6	39.8	1.8	2.4
32.8	55.6	500	31.0	31.1	-0.1	0.7
32.8	55.6	530	30.1	29.8	0.3	0.3
32.8	55.6	560	28.6	28.6	0.0	0.8
32.8	75.7	500	25.8	24.7	1.1	1.0
32.8	75.7	530	22.2	23.6	-1.4	1.8
32.8	75.7	560	22.0	22.6	-0.6	1.8
32.8	87.1	500	60.8	54.3	6.5	10.6
32.8	87.1	530	55.6	52.9	2.7	6.4
32.8	87.1	560	45.8	51.4	-5.6	5.0

Appendix C-6. LiBr-KBr-LiF Eutectic (LM#2) Electrolyte/30% MgO

Pressure	% Theor. Density	Temp.	Obs. % Change ($\bar{Y}$)	Est. % Change $\hat{Y}$	Diff. $\bar{Y}-\hat{Y}$	Std. Dev. (S)
14.4	55.4	500	18.0	17.7	0.3	0.4
14.4	55.4	530	17.2	17.2	0.0	0.1
14.4	55.4	560	16.0	16.7	-0.7	0.7
14.4	75.5	500	11.4	9.1	2.3	1.4
14.4	75.5	530	10.6	8.7	1.9	1.1
14.4	75.5	560	8.8	8.4	0.4	1.9
14.4	84.5	500	8.9	9.2	-0.3	1.6
14.4	84.5	530	7.5	8.9	-1.4	2.0
14.4	84.5	560	7.5	8.6	-1.1	0.2
23.8	55.4	500	19.5	19.5	0.0	0.3
23.8	55.4	530	18.7	18.9	-0.2	0.5
23.8	55.4	560	18.0	18.4	-0.4	0.7
23.8	75.5	500	10.9	11.3	-0.4	0.2
23.8	75.5	530	11.2	10.9	0.3	1.5
23.8	75.5	560	10.7	10.5	0.2	1.0
23.8	84.5	500	10.0	12.0	-2.0	1.1
23.8	84.5	530	13.6	11.6	2.0	1.9
23.8	84.5	560	9.2	11.2	-2.0	0.4
32.8	55.4	500	21.2	21.4	-0.2	0.7
32.8	55.4	530	21.0	20.7	0.3	0.2
32.8	55.4	560	20.9	20.1	0.8	0.2
32.8	75.5	500	12.5	13.8	-1.3	1.1
32.8	75.5	530	11.2	13.4	-2.2	1.1
32.8	75.5	560	12.6	12.9	-0.3	1.4
32.8	84.5	500	16.0	15.3	0.7	1.9
32.8	84.5	530	16.2	14.8	1.4	0.4
32.8	84.5	560	16.2	14.4	1.8	1.6

Appendix C-7. LiCl-LiBr-LiF Eutectic (All-Li) Electrolyte/30% MgO

Pressure	% Theor. Density	Temp.	Obs. % Change ($\bar{Y}$)	Est. % Change $\hat{}$ ($\hat{Y}$)	Diff. $\hat{}$ ($\bar{Y}-\hat{Y}$)	Std. Dev. (S)
14.4	60.0	500	33.5	33.6	-0.1	0.4
14.4	60.0	530	33.8	32.1	1.7	0.6
14.4	60.0	560	31.0	30.7	0.3	0.4
14.4	75.5	500	29.0	31.2	-2.2	0.7
14.4	75.5	530	26.7	29.7	-3.0	1.4
14.4	75.5	560	24.6	28.3	-3.7	1.8
14.4	85.2	500	36.8	35.9	0.9	0.6
14.4	85.2	530	36.0	34.4	1.6	1.2
14.4	85.2	560	36.1	32.9	3.2	3.9
23.8	60.0	500	41.3	42.1	-0.8	1.4
23.8	60.0	530	40.2	40.5	-0.3	0.6
23.8	60.0	560	38.8	38.9	-0.1	0.9
23.8	75.5	500	40.3	39.9	0.4	0.7
23.8	75.5	530	37.6	38.3	-0.7	1.3
23.8	75.5	560	37.5	36.7	0.8	0.8
23.8	85.2	500	44.9	45.5	-0.6	0.8
23.8	85.2	530	44.0	43.8	0.2	0.4
23.8	85.2	560	44.0	42.1	1.9	2.4
32.8	60.0	500	52.4	52.2	0.2	0.8
32.8	60.0	530	50.1	50.5	-0.4	1.2
32.8	60.0	560	47.3	48.9	-1.6	1.4
32.8	75.5	500	52.4	50.5	1.9	0.7
32.8	75.5	530	51.9	48.8	3.1	1.7
32.8	75.5	560	47.1	47.1	0.0	1.8
32.8	85.2	500	55.4	56.4	-1.0	0.8
32.8	85.2	530	53.8	54.8	-1.0	1.2
32.8	85.2	560	52.3	53.1	-0.8	1.5

Appendix C-8. LiCl-LiBr-LiF Eutectic (All-Li) Electrolyte/35% MgO

Pressure	% Theor. Density	Temp.	Obs. % Change ($\bar{Y}$)	Est. % Change $\hat{Y}$	Diff. ($\bar{Y}-\hat{Y}$)	Std. Dev. (S)
14.4	57.5	500	29.9	30.4	-0.5	0.3
14.4	57.5	530	29.5	29.3	0.2	0.7
14.4	57.5	560	28.2	28.2	0.0	0.9
14.4	75.4	500	19.5	17.0	2.5	3.9
14.4	75.4	530	16.8	16.3	0.5	1.2
14.4	75.4	560	14.7	15.6	-0.9	0.7
14.4	85.0	500	21.7	21.2	0.5	1.8
14.4	85.0	530	21.3	20.3	1.0	2.1
14.4	85.0	560	23.7	19.5	4.2	5.2
23.8	57.5	500	32.4	32.4	0.0	0.1
23.8	57.5	530	31.7	31.3	0.4	0.6
23.8	57.5	560	31.2	30.2	1.0	1.2
23.8	75.4	500	25.0	24.7	0.3	0.7
23.8	75.4	530	23.4	23.8	-0.4	0.8
23.8	75.4	560	20.9	22.8	-1.9	1.0
23.8	85.0	500	34.6	34.4	0.2	3.9
23.8	85.0	530	37.5	33.3	4.2	4.6
23.8	85.0	560	34.1	32.2	1.9	4.5
32.8	57.5	500	37.6	38.1	-0.5	0.4
32.8	57.5	530	36.6	36.9	-0.3	0.9
32.8	57.5	560	35.8	35.8	0.0	0.7
32.8	75.4	500	39.8	37.7	2.1	2.4
32.8	75.4	530	37.6	36.5	1.1	1.7
32.8	75.4	560	36.1	35.3	0.8	0.5
32.8	85.0	500	51.1	54.0	-2.9	3.3
32.8	85.0	530	48.8	52.7	-3.9	4.7
32.8	85.0	560	47.5	51.4	-3.9	4.2

Unlimited Distribution

2 Wright Laboratory
Aero Propulsion and Power Directorate
Att: R. A. Marsh
D. M. Ryan
WL/POOS-2
1950 Fifth St.
Wright-Paterson AFB, OH 45433-7251

4 Argonne National Laboratory
Chemical Technology Div.
Attn: D. Vissers
L. Redey
J. Smaga
T. Kaun
9700 South Cass Ave.
Argonne, IL 604339

2 Army Materials and Mechanism
Research Center
Attn: J. W. McCauley
P. Wong
Watertown, MA 02172

2 Army Research Lab
Attn: F. Krieger
A. Goldberg
2800 Powder Mill Road
Adelphi, MD. 20783

1 A. A. Benderly, Consultant
9915 Logan Dr.
Potomac, Maryland 20854

3 Boeing Aerospace
Attn: C. Johnson
J. Kavandi
Sid Gross
P. O. Box 3999
Seattle, WA 98124

5 Eagle-Picher Industries, Inc.
Electronics Div. Couples Dept.
Attn: R. Spencer
F. Smith
J. DeGruson
R. Hudson
J. Wells
P.O. Box 47
Joplin, MO 64802

2 General Dynamics Pomona Div.
Attn: Kathy Wong
Jaime Perez
Mail Zone 4-66
P. O. Box 2507
Pomona, CA 91769-2507

1 Hughes Aircraft Co.
Attn: L. A. Schaum, Jr.
Building 803
Mail Station E
P. O. Box 11337
Tuscon Az. 85721

1 Martin-Marietta
Specialty Components Div.
Attn: W. McCracken
P.O. Box 2908
Largo, FL 34649

1 Naval Ordnance Station
Attn: K. Englander
Code 5123C
Indian Head, MD 20640

2 Naval Sea Systems Command
Attn: F. Butler
M. F. Murphy
Attention Code SEA63R-32
Washington, DC 20235

2 Naval Surface Warfare Center
Attn: B. Larrick
C. E. Mueller
Silver Springs, MD. 20910

1 Naval Surface Warfare Center
Attn: C. Winchester
Code R33
10901 New Hampshire Ave.
Silver Spring, MD 20903-5000

1 Naval Underwater Systems Center
Attn: R. S. Lazar
Code 36301
Newport, RI 02840

3 Naval Weapons Center
Attn: M. H. Miles
R. Nolan (Code 3626)
D. Rosenlof (Code 3626)
China Lake, Ca 93555

1 Parker Hannifin
Attn: Arvind Ahluwalia, MS K141
14300 Alton Parkway
Irvine, CA 92718-1814

2 SAFT America
Attn: K. K. Press
J. Embrey
107 Beaver Court
Cockeysville, MD 21030

1 Technochem Co.
Attn: Shyam Argade
203A Creekridge Rd.
Greensboro, NC 27406

2 Defence Research Agency
Materials Dept.
Attn: J. Knight
A. G. Ritchie
Building R178
Farnborough
Hants GU14 6TD
ENGLAND

1 Leclanche, S.A.
Attn: P. Reutschi
48, Avenue de Grandson
CH-1401 Yverdon-Les-Bain
SWITZERLAND

1 0614 A. H. Andazola, 2222
1 0614 J. A. Gilbert, 2222
1 0614 K. R. Grothaus, 2222
10 0614 R. A. Guidotti, 2223
1 0614 F. P. Lasky, 2222
1 0614 L. M. Moya, 2222
1 0614 F. W. Reinhardt,2223
1 0614 G. L. Scharrer, 2223
5 0829 E. V. Thomas, 12323
1 9018 Central Technical Files, 8523-2
5 0899 Technical Library, 13414
1 0619 Print Media, 12613
2 0100 Document Processing, 7613-2
For DOE/OSTI